Longitudinal Multimode Dynamics in Monolithically Integrated Master Oscillator Power Amplifiers

Antonio PEREZ-SERRANO [(1)], Mariafernanda VILERA [(1)], Julien JAVALOYES [(2)], Jose Manuel G. TIJERO [(1)], Ignacio ESQUIVIAS [(1)] and Salvador BALLE [(2,3)]

1. CEMDATIC-E.T.S.I. Telecomunicación, Universidad Politécnica de Madrid (UPM), 28040 Madrid, Spain.
2. Departament de Física, Universitat de les Illes Balears (UIB), 07122 Palma de Mallorca, Spain.
3. Institut Mediterrani d'Estudis Avançats (IMEDEA), CSIC-UIB, 07190 Esporles, Spain.

Contact name: Antonio Pérez-Serrano (antonio.perez.serrano@upm.es).

ABSTRACT:

We theoretically investigate a dynamical regime, experimentally observed in monolithically integrated master oscillator power amplifiers emitting at 1.5 μm, consisting in large emission wavelength jumps of the device from the Bragg wavelength to that of the gain peak. Our analysis is based on numerical simulations by means of a travelling wave model that incorporates spatial effects such as spatial hole burning and coupled-cavity effects. Thermal effects are included by considering the optical response of the quantum well active medium within the quasi-equilibrium approximation at finite temperature, with a phenomenological description of the redshift of the gain peak and the changes in the background material refractive index by means of self- and cross-heating coefficients for both sections. We find that whereas the thermally-induced index changes are the responsible of the modal jumps between consecutive modes, the carrier-induced refractive index changes are the responsible of the jumps occurring between the Bragg wavelength and the gain peak.

Key words: semiconductor lasers, master oscillator power amplifier, multimode dynamics, thermal effects

1.- Introduction

Monolithically integrated Master Oscillator Power Amplifiers (MOPAs) are semiconductor-based devices suitable for applications requiring high brightness light sources (those with output powers from hundreds of mW to a few W and beam quality factor $M^2 < 3$). In addition, MOPAs are promising candidates to be modulated at high speed, as required for applications such as LIDAR, free space optical communications and laser projection displays [1]. Monolithically integrated MOPAs usually comprise two sections: an index guided single lateral mode waveguide section (a Distributed Feedback (DFB) laser in our case) that acts as a Master Oscillator (MO) and a gain-guided tapered Power Amplifier (PA) section. Ideally, the single lateral and longitudinal mode generated by the MO is injected into the PA section where it undergoes free diffraction and amplification keeping its initial beam quality. However, MOPAs often exhibit instabilities that have been attributed to a combination of thermal effects and the residual reflectance at the amplifier front facet, leading to coupling of the MO modes and the modes of the full MOPA cavity [2,3].

Here we theoretically investigate a dynamical regime, experimentally observed in a MOPA emitting at 1.5 μm [3]. The main feature of this regime is the large emission wavelength jumps occurring for low currents in the MO section as a quasi-periodic function of the CW current in the PA section. The theoretical framework is a Travelling Wave

Model (TWM) [4] that naturally includes spatial effects (such as Spatial Hole Burning (SHB) and coupled-cavity effects) and multimode dynamics. Thermal effects are included by considering the optical response of the Quantum Well active medium within the quasi-equilibrium approximation at finite temperature [5]. The redshift of the gain peak and the changes in the background material refractive index are phenomenologically included in the model by thermal coefficients accounting for the self- and cross-heating effects of both sections. Although a full description of the MOPA dynamics requires at least a 2-D spatial model [2,6] in order to address the possible filamentation in the PA section, good qualitative agreement has been obtained between the experiments and a 1-D TWM [7], showing that the wavelength jumps arise mainly from the interplay of longitudinal modes and thermal effects. In this contribution we further investigate theoretically the physical mechanisms involved in the observed dynamics. In particular we focus our analysis on the role of the thermal effects and the carrier-induced effective index changes. We find that as the PA current is varied, the thermally-induced index changes are responsible for the switching between consecutive longitudinal modes; however, the large jumps from the Bragg wavelength to the PA gain peak stem from the carrier-induced changes in the effective refractive index.

2.- The travelling wave model

In this section we briefly summarize the 1-D TWM developed in [4,8] that was suitably modified in [7] in order to phenomenologically include the thermal drift of the material properties in each section. We consider a two-section device. Within each section *j*, an optical field with optical carrier frequency ω_0 and effective propagation constant q_0 is decomposed into a forward and a backward components which slowly-varying amplitudes, $E_j^{\pm}$, propagate according to

$$\pm\partial_z E_j^{\pm} + \frac{1}{v_g}\partial_t E_j^{\pm} = \left[i\delta_j(T_j) - \alpha_i\right]E_j^{\pm} + i\kappa_j^{\pm}E_j^{\mp} + iP_j^{\pm}, \quad (1)$$

where the amplitudes and material variables have been suitably scaled. α_i is the amplitude absorption coefficient, v_g is the group velocity, $\kappa_j^{\pm}$ is the coupling coefficient of the Bragg grating in section *j*, if any. We take the optical carrier wavelength ω_0 as that corresponding to the Bragg wavelength in the MO. $\delta_j(T_j)$ is the thermally induced change of the effective refractive index that induces a detuning with respect to ω_0. The detuning depends on the temperature of the section as

$$\delta_j(T_j) = \frac{\delta n_g}{\delta T}\frac{\Delta T_j}{L_j}, \quad (2)$$

where $\delta n_g/\delta T$ is the coefficient of thermal change in the effective group index, L_j is the section length and ΔT_j is the temperature change within the section.

In a similar way, the carrier density is decomposed as $N_j(z,t) = N_j^0(z,t) + N_j^+ e^{2iq_0z} + N_j^- e^{-2iq_0z}$, where N_j^0 is the quasi-homogenous component and $N_j^{\pm}$ (with $N_j^- = (N_j^+)^*$) are the spatial grating components arising from SHB due to the standing-wave effects in the section. These obey

$$\pm\partial_t N_j^0 = \frac{I_j}{s_j} - R_j(N_j^0) - i(E_j^{+*}P_j^+ + E_j^{-*}P_j^- - c.c.), \quad (3)$$

and

$$\pm\partial_t N_j^{\pm} = -\left[R'_j(N_j^0) + 4D_j q_0^2\right]N_j^{\pm} - i(P_j^{\pm}E_j^{\mp *} - E_j^{\pm}P_j^{\mp *}), \quad (4)$$

where I_j is the current injected into the section, s_j is a scale factor taking into account the volume of the different sections, $R_j(N) = A_jN + B_jN^2 + C_jN^3$ is the carrier recombination in the section, $R'_j(N) = d_N R_j(N)$, $4D_jq_0^2$ is the decay rate of the grating terms due to carrier diffusion, and the remaining terms describe stimulated recombination. The polarization densities $P_j^{\pm}$, which describe the gain and carrier-induced refractive index, are given by [8]

$$P_j^{\pm} = \chi_0 \int_0^{\infty} dt' \left\{ \chi_j\left[t', N_j^0(t', r)\right] E_j^{\pm}(z, r) + N_j^{\pm}(z, r) \frac{\partial \chi_j\left[t', N_j^0(r)\right]}{\partial N_j} E_j^{\mp}(z, r) \right\} + \eta \xi_j^{\pm}(z, t) \quad (5)$$

where $r = t - t'$ and spontaneous emission is taken into account by including a Gaussian white noise term $\xi_j^{\pm}(z,t)$. The convolution kernel

$$\chi_j(t', N_j) = \frac{e^{-\left[\gamma + i\left(\Omega_{Gj} - w_0\right)\right]t'}}{t'} \left(2e^{-i\gamma N_j t'} - 1 - e^{-i(\Omega_T - \Omega_{Gj})t'}\right) \quad (6)$$

describes the optical response of the material in time domain under the intraband quasi-equilibrium approximation, which is valid in time scales of 1 ps and longer. We describe phenomenologically the thermally induced redshift of the material gain peak considering

$$\Omega_{Gj} = \Omega_G^0 - c_j \Delta T_j. \quad (7)$$

The temperature in each section is described via self- and cross-heating coefficients [2]

$$\begin{pmatrix} \Delta T_{MO} \\ \Delta T_{PA} \end{pmatrix} = \begin{pmatrix} \theta_{11} & \theta_{12} \\ \theta_{21} & \theta_{22} \end{pmatrix} \begin{pmatrix} P_{MO} \\ P_{PA} \end{pmatrix}, \quad (8)$$

where the diagonal elements (θjj) are the self-heating coefficients and the non-diagonal ones describe cross-heating (θij). $P_j = P_j^{elect} - P_j^{opt}$ is the power dissipated within the section, which is a function of the difference between the injected electrical power and the optical output. Noting that 1.5 µm devices have a low output efficiency, the optical power is negligible as compared to the electrical power, thus simplifying considerably the simulations.

Finally the TWM is closed by specifying the boundary conditions

$$\begin{cases} E_{MO}^{+}(0,t) = r_0 E_{MO}^{-}(0,t) \\ E_{MO}^{-}(z_1,t) = r_1 E_{MO}^{+}(z_1,t) + t_1' E_{PA}^{-}(z_1,t) \\ E_{PA}^{+}(z_1,t) = r_1' E_{PA}^{-}(z_1,t) + t_1 E_{MO}^{+}(z_1,t) \\ E_{PA}^{-}(z_2,t) = r_2 E_{PA}^{+}(z_2,t) \end{cases} \quad (9)$$

where $z_1 = L_{MO}$, $z_2 = L_{MO} + L_{PA}$, r and t are the reflection and transmission coefficients as sketched in Fig. 1.

In summary, our TWM considers two separate sections with different temperatures and biasing points. Compound-cavity effects arise from the optical coupling of the MO and PA sections. Within each section, the local carrier density determines the gain and carrier-induced index spectra; the temperature of the section determines the local band gap energy and the effective index of the section. These two effects lead to changes in wavelength and net gain of the cavity modes when the bias currents are varied through self- and cross-heating. We refer the reader to [7] for more details and parameter values.

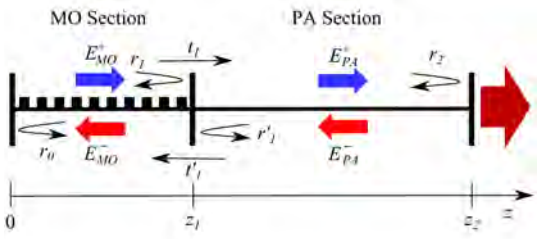

Fig. 1: Boundary conditions for the electric fields $E_j^{\pm}$. r_0, r_1, r_1', r_2 and t_1, t_1' are the reflection and transmission coefficients for the fields amplitudes. $z_1 = L_{MO}$ and $z_2 = L_{MO} + L_{PA}$.

2.- Results

Here we focus on the conditions where the large wavelength jumps appear, i.e. having biased the MO close to its threshold while increasing the current in the PA. Fig. 2 shows qualitatively good agreement with the behavior reported in [3]. Fig 2 (a) shows the optical spectra in two panels for different wavelength ranges. The MOPA threshold occurs for I_{PA} ~ 0.7 A, and the lasing wavelength corresponds to that of the Bragg grating in the MO section.

As the current in the PA section is increased, the emission wavelength exhibits a small redshift due to the thermal drift of the Bragg wavelength as the refractive indexes increase due to cross-heating. Further increasing the PA current the optical spectrum of the device changes dramatically, passing from narrow emission at the Bragg wavelength to broadband emission at a much shorter wavelength that corresponds to that of the material gain peak in the PA section. In this regime the RF spectrum (Fig. 2 (b)) displays strong peaks at

f = 17 GHz and 34 GHz, which correspond to the Free Spectral Range (FSR) of the full MOPA cavity. Continuing increasing the PA current the wavelength jumps occur in a quasi-periodic way.

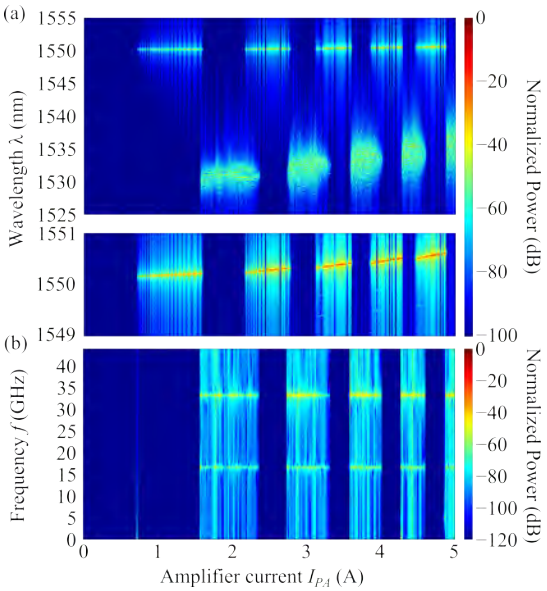

Fig. 2: Results for I_{MO} = 54 mA while varying I_{PA}. (a) Optical and (b) RF spectra.

In order to get a deeper physical insight, the role of the thermal effects and the carrier-induced effective index changes are separately investigated. The carrier-induced effective index changes are neglected by setting $\mathrm{Re}\{\chi_j\}$ = 0 in Eq. (6) whereas the effect of the thermal redshift of the material gain (Eq. (7)) is kept, and the coefficient of thermal change in the effective group index $\delta n_g/\delta T$ is set to zero or 10^{-4} K^{-1}. Fig. 3 shows the results for simulations using the parameter set of Fig. 2 except for those indicated in the legend. The cases are ordered from less to more effects, being the case with all the effects taken into account shown in Fig. 2. As shown for case 1, when $\delta n_g/\delta T$ is set to zero and the carrier-induced index changes are neglected, the laser emits at the Bragg wavelength (around 1550 nm) for the whole I_{PA} range. The RF spectrum for this case shows only relaxation oscillations at a few GHz. The situation changes completely when the carrier-induced index changes are taken into account as shown in Fig. 3 case 2. In this case for I_{PA} > 1.2 A emission at the gain peak of the PA section appears together with emission at the Bragg wavelength. While varying I_{PA}, a 5 nm displacement of the gain of the PA section due to the thermal redshift of the band-gap energy can be observed. In this situation the RF spectrum shows peaks corresponding to the FSR of the full MOPA cavity.

Fig. 3 case 3 shows the optical and RF spectra when $\delta n_g/\delta T \neq 0$, the cross-heating coefficients θij = 0 and $\mathrm{Re}\{\chi_j\}$ = 0. In this case the Bragg wavelength does not drift but the emission mode changes as a consequence of the self-heating of the PA section. Wavelength jumps between consecutive modes similar to those reported in [2] are found as a consequence of the drift of the modes while the Bragg wavelength keeps constant around 1550 nm. Finally, when cross-heating is allowed ($\theta ij \neq 0$) and only $\mathrm{Re}\{\chi_j\}$ is set to zero (case 4), both the Bragg wavelength and the modes of the full MOPA cavity shift as a function of I_{PA}. However, the amount of these shifts is different and this leads to less wavelength jumps than in the previous case. In both cases no emission at the gain peak of the PA section appears and the RF spectra show relaxation oscillations peaks at a few GHz when the modal jumps take place.

The above results reveal two main facts: On one hand, the quasi-periodic jumps are a consequence of the thermal effects, in particular to the temperature induced refractive index changes in each section, and the position of these jumps is given by the interplay between the thermal drifts of the modes of the full MOPA cavity and the Bragg wavelength. On the other hand, the emission at the gain peak of the PA section should be attributed to the carrier-induced effective index changes. In our material description, Eq. (5) provides the gain and carrier-induced refractive index. The linewidth enhancement factor or α-factor is implicit in our description and depends on the wavelength. The difference between the α-factor values at the Bragg wavelength and at the gain peak wavelength of the PA section allows for the emission either at both wavelengths or at one of them depending on the position of the modes of the full MOPA cavity and the Bragg wavelength.

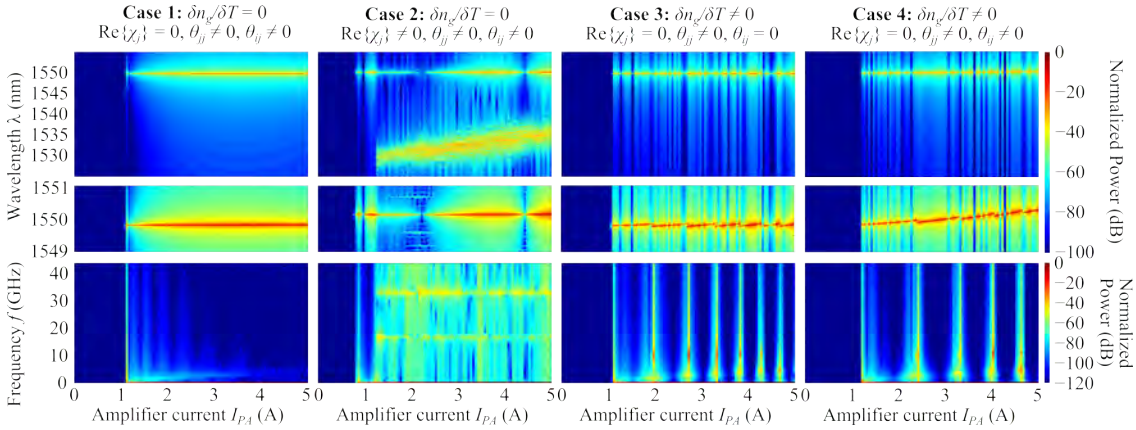

Fig. 3: Dependence on the thermal effects and the carrier-induced effective index changes for different cases distributed in columns. I_{MO} = 54 mA.

4.- Conclusion

We have theoretically analyzed the physical mechanisms involved in the large wavelength jumps observed in the spectra of integrated MOPAs working at 1.5 µm. By separately analyzing the role of the thermal effects and the carrier-induced effective index changes, we have found that the thermally-induced index changes are the responsible of the position of the modes and the jumps between consecutive modes as a function of the current in the power amplifier section. Yet, the carrier-induced refractive index changes are the responsible of the jumps occurring between the Bragg and the gain peak wavelength.

Acknowledgements: This work has been supported by the Ministerio de Economía y Competitividad of Spain through project RANGER (TEC2012-38864-C03-02 and TEC2012-38864-C03-01). A. Pérez-Serrano, M. Vilera, J.M.G. Tijero and I. Esquivias also acknowledge support from the European Commision through the project BRITESPACE under grant agreement no. 313200 and the Comunidad de Madrid under program SINFOTON-CM (S2013/MIT-2790). J. Javaloyes also acknowledges support from the Ramon y Cajal fellowship.

References

[1] P. Adamiec, B. Bonilla, A. Consoli, J.M.G. Tijero, S. Aguilera, and I. Esquivias, "High-peak-power pulse generation from monolithic master oscillator power amplifier at 1.5 µm", *Appl. Opt.* **51**, 7160 (2012).

[2] M. Spreemann, M. Lichtner, M. Radziunas, U. Bandelow, and H. Wenzel, "Measurement and simulation of distributed-feedback tapered master-oscillator power amplifiers", *IEEE J. Quantum Electron.* **45**, 609 (2009).

[3] M. Vilera, A. Pérez-Serrano, J.M.G. Tijero, and I. Esquivias, "Emission characteristics of a 1.5 µm all semiconductor tapered master oscillator power amplifier", *IEEE Photon. J.* **7**, 1500709 (2015).

[4] J. Javaloyes, and S. Balle, "Emission Directionality of Semiconductor Ring Lasers: A Traveling-Wave Description", *IEEE J. Quantum Electron.* **45**, 431 (2009).

[5] J. Javaloyes, and S. Balle, "Detuning and thermal effects on the dynamics of passively mode-locked quantum-well lasers", *IEEE J. Quantum Electron.* **48**, 1519 (2012).

[6] A. Pérez-Serrano, J. Javaloyes, and S. Balle, "Spectral Delay Algebraic Equation Approach to Broad Area Laser Diodes", *IEEE J. Sel. Topics Quantum Electron.* **19**, 1502808 (2013).

[7] A. Pérez-Serrano, M. Vilera, J. Javaloyes, J.M.G. Tijero, I. Esquivias, and S. Balle, "Wavelength Jumps and Multimode Instabilities in Integrated Master Oscillator Power Amplifiers at 1.5 µm: Experiments and Theory", *IEEE J. Sel. Topics Quantum Electron.* **21**, 1500909 (2015).

[8] J. Javaloyes and S. Balle, "Quasiequilibrium Time-domain Susceptibility of Semiconductor Quantum Wells", *Phys. Rev. A* **81**, 062505 (2010).